

Modeling and control of a soft pneumatic finger without fiber reinforcement

Triet Hung Ho^{1,2}, Le The Truyen³, Quoc Viet Luong³, Thi My Nu Ho^{3*}

¹ University of Technology (HCMUT), 268 Ly Thuong Kiet Street, District 10, Ho Chi Minh City, Vietnam

² National University Ho Chi Minh City, Linh Trung Ward, Thu Duc City, Ho Chi Minh City, Vietnam

³ Ho Chi Minh City University of Industry and Trade; 140 Le Trong Tan, Tay Thanh Ward, Tan Phu District, Ho Chi Minh City, Vietnam

* Corresponding author's e-mail: nuhtm@huit.edu.vn

ABSTRACT

Soft pneumatic actuators (SPAs) have been increasingly used as fingers in robotic hands because of their inherent compliance, cost-effectiveness, and ease of construction. Nonetheless, the efficient modeling and controlling of soft pneumatic actuators is challenging due to inherent hysteresis nonlinearity, uncertainties, and external environmental perturbations. Another challenge in controlling soft mechanisms is the need for bending angle feedback signals from curvature sensors, but integrating curvature sensors into soft mechanisms is difficult and increases manufacturing costs. This paper proposes a simpler approach to controlling soft mechanisms. Instead of using the bending angle feedback signal from the curvature sensor, this study proposes a bending angle control solution through pressure. The analytical models for both the soft finger and pneumatic valves have been constructed. Subsequent bending tests are performed to ascertain the relationship between bending angle and air pressure. This work analyzes the adaptive sliding mode utilizing active rejected control to regulate the position of the soft pneumatic finger. The suggested control approach integrates parametric uncertainty and input constraints to mitigate the effects of system uncertainties. The simulation results reveal modest overshoots and little steady-state errors in the actuator's response; hence, the proposed controller has effectively fulfilled its control function. Comprehending soft material actuators devoid of curvature sensors would facilitate the rapid replication of novel design concepts and enable estimations of their efficacy without reliance on curvature sensors. This will result in more applications and the development of increasingly intricate motion systems.

Keywords: soft robot, pneumatic system, robotics, active rejected control, sliding mode control.

INTRODUCTION

Soft robotics has emerged as a leading concern within the robotics community, and the surge in academic research on the topic illustrates its transformative potential in societal institutions and many industries. Many practical applications where the highly dynamic environment or sensitivity to physical interaction for soft robots have been proposed including grippers and manipulators [1], human-machine interactive and wearable devices [2, 3], smart sensors [4], and so on. Recently, a promising domain utilizing soft mechanisms is the study of collaborative robotics.

Robots have generally been prohibited from engaging with people due to safety concerns [5]. A collision between a stiff robot and a person may result in injuries. Nevertheless, soft robots may engage in collaborative interactions with people without doing any damage. Consequently, they are employed in several industrial and medical applications to assist human operators in a safer manner [6, 7]. Various types of soft robots have been developed such as magnetic soft robots [8], mechanical instabilities [9, 10], thermally responsive soft robots [11], and electrically responsive soft robots [12]; however, pneumatic soft robots remain the dominant technology in soft robotics

due to its lightweight, fast response time, and easy implementation [13],

Two main types of pneumatic soft robots, with and without fiber reinforcement pneumatic soft robots, have been successfully investigated through experiments or simulations. For example: Xie *et al.* [14] adopt a 3D pneumatic soft actuator without fiber reinforcement or omni-directional soft pneumatic actuators. The paper produced the finite element model (FEM) and basic control for air pressure. Xavier *et al.* [15] produced the FEM and compare it with the experimental results of the omni-directional soft pneumatic actuators. Fionnuala Connolly *et al.* [16], developed the analytical modeling of a fiber reinforcement soft pneumatic actuators that can expand, twist, and bend. Guoliang Zhong *et al.* [17] investigated a theory model of a bending angle and contact force of a pneumatic soft actuator with pleated structures reinforcement. The fiber-reinforced pneumatic soft robot discussed in the aforementioned research has several components, rendering its fabrication challenging.

The production procedure of non-fiber-reinforced soft robots is more streamlined than that of fiber-reinforced pneumatic soft robots. However, the mathematical modeling of this sort of pneumatic soft robot is complex due to significant variations in the geometrical dimensions of the pneumatic chamber, resulting from the material's elasticity. So, the analytical model and controller for the pneumatic soft robot system remain undeveloped. The majority of the research above shows that in order to implement the controller, it is necessary to get both bending angle and pressure feedback signals. Researchers have devised methods for integrating curvature sensors into soft actuators to resolve this problem. Given the significant deformation the soft mechanism undergoes during operation, embedded sensors must exhibit a high degree of elasticity and flexibility. As a result, these integrated sensors must exhibit high reliability and endurance, leading to increased production costs. Moreover, the incorporation of curvature sensors is crucial, as it complicates the design and manufacturing processes when these soft actuators operate as modules inside soft robots, which include several such components. Furthermore, it is crucial to recognize that radial deformations may alter the linear correlation between the axial deformation associated with the bending angle and the output voltage. Consequently, their conventional operation relies

on the absence of overlap between axial and radial deformations a condition that is difficult to provide when the soft actuator demonstrates overlapping and complex deformations. In order to make the manufacturing process more efficient and get the most out of soft actuators, a soft mechanism that doesn't need the bending sensors to work must be created. To realize this concept, it is important to have a dynamic model that accurately determines the relationship between the input pressure and the bending angle. This model needs to consider the hyperelastic properties of the silicone rubber, the geometry of the actuator, and the appropriate control solution derived from the dynamic model.

This study develops a pneumatic soft finger in hand robot without fiber reinforcement and without an integrated curvature sensor. Instead of using the bending angle feedback signal from the curvature sensor, this study proposes a dynamic model that accurately describes the relationship between the bending angle and the pneumatic pressure. This relationship enables pressure control to achieve the desired bending angle. We construct a dynamic model for both the soft robot and the pneumatic valve to effectively control the pneumatic pressure. To keep track of the changes in the bending angle, an adaptive sliding mode controller combined with an active reject disturbances control is used. This is because the internal model of the pneumatic soft robot system is not linear, uncertain, and unstable. We conduct simulations to showcase the effectiveness of the proposed solution.

MATHEMATICAL MODEL OF SOFT FINGER WITH SINGLE AIR CHAMBER

The bending angle is the most important parameter in order to verify the effectiveness of a pneumatic soft robot finger [18]. According to Bernoulli-Euler theory [19], if a constant moment (M) applies to a beam, the bending angle is approximately constant, as can be seen in Figure 1. The relationship between the radius of the bending angle (R_A), Young's modulus (E), and the moment of inertia (I) is given by:

$$\theta = \frac{l^*}{R_A} \quad (1)$$

Assume that the bending angle θ with constant, as can be seen in Figure 1, so it can be calculated as:

Assume that the bending angle θ with constant, as can be seen in Figure 1, so it can be calculated as:

$$\theta = \frac{l^*}{R_A} \tag{2}$$

where: l^* is the final length of air chamber of the finger under the air pressure. Under the air pressure p , the relationship between the force and cross-section area a of air chamber is shown below:

$$F = pa \tag{3}$$

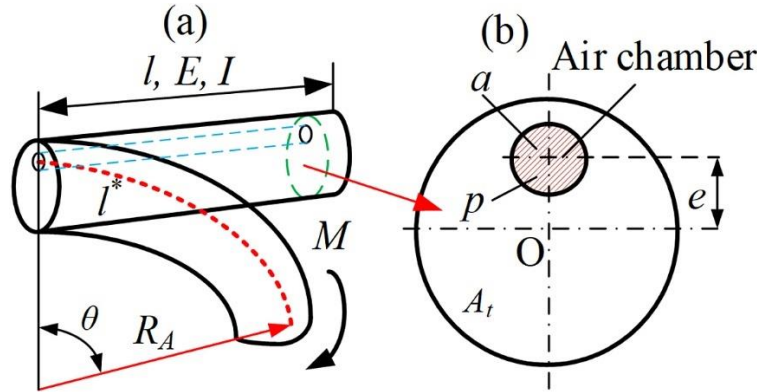


Figure 1. Proposed soft actuator finger with single air chamber:
(a) Bending angle model, (b) Cross-section

If the neutral axis of the cross-section passes through the center of pressure, the soft finger uniformly expands in all directions and it will not bend. The soft finger in this study is made to have a slight difference e between the center of compression pressure p and the center of gravity O of the body's cross-sectional area; as a result, when compressed air pressure is applied, the actuator will bend in that direction. The pulling force F times the deflection e between the center of pressure and the neutral axis equals the moment that results in this bending, as:

$$M = Fe = pae \tag{4}$$

If the normal stress that develops as a result of the tensile force F is smaller than the material's elastic deformation, the deformation along the length of the actuator is calculated as follows:

$$\Delta l = \frac{Fl}{A_t E} = \frac{pal}{A_t E} \tag{5}$$

where: A_t is the cross-area of the body and l is the initial length before deformation. Combine Equation 1 and Equation 4, we got:

$$\frac{1}{R_A} = \frac{pae}{EI} \tag{6}$$

When the soft robot reaches the stable state, the final length of the air chamber is given by:

$$l^* = l + \Delta l \tag{7}$$

Replacing Equations 5, 6 and 7 into Equation 2, we got:

$$\theta = \frac{l^*}{R_A} = \frac{l + \Delta l}{R_A} = \frac{pae}{EI} \left(l + \frac{pal}{A_t l} \right) \tag{8}$$

Simplifying the Equation 8, the relationship between air pressure and bending angle is given

$$\theta = \mu_1 p^2 + \mu_2 p \tag{9}$$

$$\mu_1 = \frac{a^2 el}{EI^2 A_t} \quad \mu_2 = \frac{ael}{EI} \tag{10}$$

Equation 9 illustrates the model dynamics, depicting the correlation between bending angle and pressure while accounting for the size of the actuator finger and characteristics of the hyperelastic material. The constants of Equation 9 are positive values, so the angle θ increases as pressure p increases. From Equation 9, we can interpolate the pressure value corresponding to the desired bending angle.

THE MODELING OF AIR COMPRESSION

Air compression system

The pressure in the air chamber of the soft finger must be controlled appropriately for the configuration facility to attain the correct angle. The air compression diagram of the air chamber is shown in Figure 2.

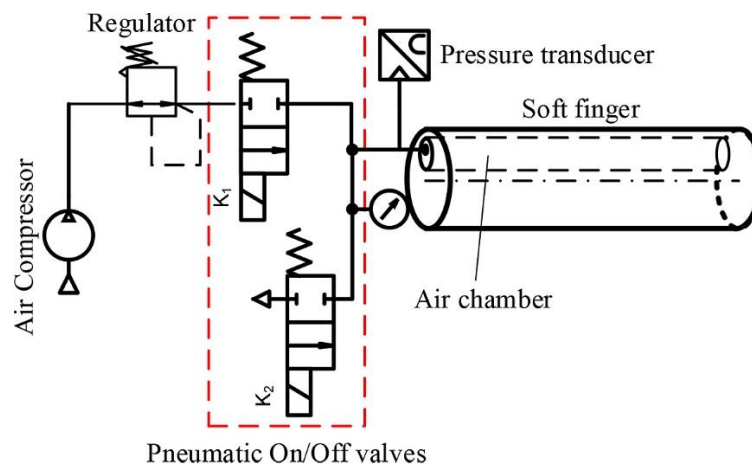


Figure 2. Diagram of compression air for soft finger with single air chamber

To reduce the cost of equipment, this air compression system uses two ON/OFF pneumatic valves that can work at high frequencies to adjust the compressed air. In this system, valve K_1 is connected to the supply application to create positive pressure, while valve K_2 is connected to the air application to release air from the soft actuator. Each valve has two states: the open state is set up to allow compressed air to pass through the valve, and the closed state is to block the flow of compressed air. A pressure sensor is installed to sense compressed air pressure in the air chamber. The signal from this sensor is provided to the controller. The valve system is mutually exclusive, preventing simultaneous air injection and expulsion. Pressure regulator valve is used to control the supply pressure.

The mathematical model

The energy equation of compressed air with pressure p , volume V , density ρ , input temperature T_{in} , and output temperature T_{out} , can be described as [20]:

$$\dot{U} = q_{in} - q_{out} + kC_v(\dot{m}_{in}T_{in} - \dot{m}_{out}T_{out}) - \dot{W} \tag{11}$$

where: q_{in} and q_{out} are heat transfer, k is conductivity, C_v is molar heat capacity at constant volume, \dot{W} is work done. The heat transfer rate can be calculated by:

$$\dot{U} = C_v \dot{m} \Delta T \tag{12}$$

where: $C_v = \frac{R_{special}}{k-1}$. The continuous compressed air mass equation is given by:

$$\dot{m} = \dot{\rho}V + \rho\dot{V} \tag{13}$$

Moreover, assuming that ideal gas is used, the ideal gas law is given:

$$p = \rho R_{special}T \tag{14}$$

where: $R_{special}$ is a special gas constant. Replace Equations 12 and 13 into Equation 14, we get:

$$\dot{U} = \frac{1}{(k-1)}(\dot{p}V - p\dot{V}) \tag{15}$$

Work done is defined as:

$$\dot{W} = p\dot{V} \tag{16}$$

Replace Equations 15 and 16 into Equation 11, we got:

$$q_{in} - q_{out} + \frac{k}{k-1} \frac{p}{\rho T} (\dot{m}_{in}T_{in} - \dot{m}_{out}T_{out}) - \frac{k}{k-1} p\dot{V} = \frac{1}{k-1} V\dot{p} \tag{17}$$

Assume that the progress is isothermal process ($T = T_{in} = T_{out}$), polytrophic process ($q_{in} = q_{out}$), the Equation 17 becomes:

$$\dot{p} = k \frac{R_{special}T}{V} (\dot{m}_{in} - \dot{m}_{out}) - k \frac{p}{V} \dot{V} \tag{18}$$

where: the volume of the air chamber is calculated by:

$$V = A \cdot l^*, \dot{V} = A \cdot \Delta \dot{l} \tag{19}$$

From the above equation it can be deduced that for a compressed air chamber, pressure is the output that depends on the input which is the mass flow of the compressed air stream. The pneumatic valve used in this study is either fully closed or fully open. The mass flow of the compressed air stream and the compressed air pressure achieved control of the opening and closing time of the pneumatic valves. The static mass flow rate of the compressed air stream when the valve is fully open is calculated according to ISO 6358 standard as follows [21]:

$$\dot{m}_{in}(p_{up}, p_{down}) = \begin{cases} p_{up} C_r \rho \sqrt{T_0/T_u} \text{ if } \frac{p_{down}}{p_{up}} \leq b_r \\ p_{up} C_r \rho \sqrt{T_0/T_u} \sqrt{1 - \frac{\left(\frac{p_{down}}{p_{up}} - b_r\right)^2}{(1 - b_r)^2}} \text{ if } \frac{p_{down}}{p_{up}} > b_r \end{cases} \tag{20}$$

where: p_{up} and p_{down} are the inlet and outlet pressures of the compressed air stream, respectively. The parameters ρ and T_0 represent the density and temperature at the reference state according to ISO 6358, T_u is the gas flow temperature, b_r is the critical pressure ratio that defines the choked flow condition and C_r is the negative conductivity. Both parameters b_r and C_r are provided by the valve manufacturer.

As shown in Figure 2, with valve #1 activated ($K_1 = 1$), compressed air will be sent to the air chamber. With valve #2 activated ($K_2 = 1$), the air in chamber will exit. Consequently, the mass flow rate for air chamber of the soft fingers denoted by Equation 21, in which q_m is mass flow as described in Equation 20 which is a function of p_{up} and p_{down}

$$\dot{m}_{in} = \begin{cases} +q_m & K_1 = 1, K_2 = 0 \\ 0 & K_1 = 0, K_2 = 0 \\ -q_m & K_1 = 0, K_2 = 1 \end{cases} \tag{21}$$

The occurrence of $(k \frac{R_{special}T}{V} (\dot{m}_{out}))$ may be ascribed to air leakage as an external disturbance represented by $-d(t)$. The Equation 18 can be simplified by:

$$\dot{y} = bu + f(t) \tag{22}$$

where:

$$b = \frac{kR_{special}T}{V}; u = \dot{m}_{in}; f(t) = -k \frac{pA}{V} (\Delta l_i) + d(t); y = p$$

It is noted that $f(t)$ represents the uncertainty vector of the direct dynamics, encompassing all vectors of uncertainties, including external disturbances.

CONTROL DESIGN

Design adaptive robust sliding mode control

The adaptive robust control problem for a category of nonlinear uncertain control affine dynamical systems, as delineated in Equation 22, entails the formulation of a control law $u(t)$ that ensures the stability of the resultant closed-loop system while tracking a specified time-varying of system states for all conceivable values of the uncertainty vector $f(t)$ across the entire state space. The sliding mode control theory is employed because of its advantageous characteristics, including resilience, excellent transient performance, and rapid response. An estimate of b , which is defined \hat{b} for this controller, will be chosen as a constant in the model. The control gain b is unknown however its limitations are established as:

$$\frac{kR_{special}T}{V_{max}} \leq b \leq \frac{kR_{special}T}{V_0} \tag{23}$$

The initial air chamber volume is V_0 , and the maximum air chamber volume is V_{max} when the actuator is not stretched. Selecting the estimate of control gain b as maximum of its boundaries, yields \hat{b} equal to $\hat{b} = \left(\frac{kR_{special}T}{V_0} \right)$. So, the equation of state in Equation 22 is rewritten as:

$$\dot{y} = \hat{b}u + f(t) \tag{24}$$

This study aims to design conservatively within the constraints of uncertainties by: (i) implementing a continuous adaptive term that can be recursively updated in an online manner to address time-varying uncertainties; (ii) incorporating a term that preserves the transient response of the closed-loop system during the learning process and compensates for errors arising from the perturbation estimation by the adaptive term. The design of the adaptive robust controller, characterized as described and without knowledge of uncertainty bounds, is undertaken through the integration of sliding mode control and systematic Lyapunov design methodologies. The two methodologies are as follows:

- a) The sliding mode control (SMC) design technique consists of two phases: (a) identifying a sliding surface to achieve the desired system performance while constrained to that surface; and developing a control law to guarantee the stability of the sliding mode.
- b) The comprehensive Lyapunov design process has three stages: (i) the selection of a control law with variable parameters or terms; (ii) the selection of an update law for modifying the variable terms; and (iii) the examination of the convergence characteristics of the constructed controller.

A sliding mode controller is formulated for the aerodynamic described in Equation 24. The sliding surface, referred to as s , and its derivative are officially defined as follows:

$$\begin{cases} s = e = p - p_r \\ \dot{s} = \dot{e} = \dot{p} - \dot{p}_r = \hat{b}u + f(t) - \dot{p}_r \end{cases} \tag{25}$$

The subsequent phase of controller design involves selecting a control rule with changeable parameters that ensures the Lyapunov function decreases with time. The subsequent control law is examined.

$$u(t) = u_{eq} + u_p + \hat{u} \tag{26}$$

where: u_{eq} , u_P and \hat{u} represents the terms of the proposed controller, defined as follows. The equivalent controlling factor u_{eq} is evaluated for the nominal system in Equation 24 in the absence of perturbations and may be formulated based on Filippov's equivalent dynamics [22], which asserts that $\dot{s} = 0$ while the dynamics operate in the sliding mode. Thus, the equivalent control law is proposed from Equation 25 as:

$$u_{eq} = \frac{1}{\hat{b}}(-f(t) + \dot{p}_r) \tag{27}$$

The feedback term u_P is a P-controller designed to augment closed-loop stability and boost transient performance during the system's learning phase. It rectifies the inaccuracy that may arise from the estimate of the perturbations and is defined as follows:

$$u_P = -\frac{1}{\hat{b}}Ks \tag{28}$$

The controller u_P is, in fact, a proportional control law for variable s , and K is positive value. The variable term \hat{u} is deemed adaptive and is formulated to counteract perturbations, defined in relation to the estimated perturbation \hat{E} as:

$$\hat{u} = -\frac{1}{\hat{b}}(\hat{E}sign(s)) \tag{29}$$

where: \hat{E} is a design parameter. Incorporating the online estimated perturbation into the control rule eliminates the necessity of utilizing uncertainty bounds. Therefore, this study proposes the subsequent control laws as:

$$u(t) = \frac{1}{\hat{b}}(-f(t) + \dot{p}_r - Ks - \hat{E}sign(s)) \tag{30}$$

Using controller $u(t)$ in Equation 30 and Equation 24 is obtained as:

$$\dot{y} = \dot{p}_r - Ks - \hat{E}sign(s) \tag{31}$$

The Lyapunov stability method is employed to examine the stability characteristics of the controller and to derive the adaptive control rule. This study proposes the Lyapunov function as follows:

$$L = \frac{1}{2}s^2 + \frac{1}{2}\left(\frac{1}{\gamma}\right)\tilde{E}^2 \tag{32}$$

where: ρ is positive definite adaptive gain, and \tilde{E} is the perturbation estimation error and is defined as:

$$\tilde{E} = \hat{E} - E \tag{33}$$

\hat{E} represents the estimated upper bound, whereas E denotes the optimum upper bound of the perturbation, both of which are positive numbers. The ideal upper limit of the perturbation is the point at which the system attains stability, hence minimizing chattering in the control signal. The objective of the design problem is to select an adaptive rule for modifying the estimate \hat{E} to ensure that s approaches zero, i.e., $\lim_{t \rightarrow \infty} s = 0$.

The derivative of the Lyapunov function, derived from Eq. (32), is:

$$\dot{L} = \dot{s}s + \left(\frac{1}{\gamma}\right)\dot{\tilde{E}}\tilde{E} \tag{34}$$

Substituting Equation 25 into Equation 34 yields:

$$\dot{L} = (\dot{p} - \dot{p}_r)s + \left(\frac{1}{\gamma}\right)\dot{\tilde{E}}\tilde{E} \tag{35}$$

Using Equations 31 and 35, we obtain:

$$\dot{L} = (-Ks - \hat{E}sign(s))s + \left(\frac{1}{\gamma}\right)\dot{\tilde{E}}\tilde{E} \tag{36}$$

Since the optimal upper bound E of perturbation is a positive constant value, from Equation 32 we get:

$$\dot{\hat{E}} = \hat{E} \tag{37}$$

Substituting Equation 33 and 37 into Equation 36 one can obtain:

$$\dot{L} = -s\hat{E}\text{sign}(s) - Ks^2 + \left(\frac{1}{\gamma}\right)\hat{E}[\hat{E} - E] \tag{38}$$

For achieving $\dot{L} \leq 0$, the estimation law is designed as follows:

$$\dot{\hat{E}} = \gamma|s| \tag{39}$$

where: γ is positive value. Substituting Equation 38 into Equation 37 yields

$$\dot{L} = -s\hat{E}\text{sign}(s) - Ks^2 + |s|[\hat{E} - E] \tag{40}$$

Since $s(\text{sign}(s)) = |s|$, then from Equation 39 we obtain:

$$\dot{L} = -Ks^2 - E|s| \leq 0 \tag{41}$$

By Barbalat’s lemma [22], it can be concluded that $s \rightarrow 0$.

Active reject disturbances control

Equation 41 illustrates that the system remains stable under the control law defined in Equation 30. The system must acquire feedback signals on the air chamber volume V of the soft finger, its derivative \dot{V} , and the boundaries of external disturbance $d(t)$ to accurately compute the value of $f(t)$. Nonetheless, accurate data on velocity and disturbance is absent in reality. This part aims to enhance the practicality of the sliding mode control system. The extended state observer (ESO) is included into the sliding mode control system to achieve this objective. This work seeks to evaluate the generalized disturbance, encompassing both velocity-related and external disturbances. The new state variables are set as follows

$$\begin{aligned} x_1 &= p \\ x_2 &= f(t) \end{aligned} \tag{42}$$

From the system Equation 22 we get:

$$\begin{aligned} \dot{x}_1 &= x_2 + bu \\ \dot{x}_2 &= h(t) \end{aligned} \tag{43}$$

where: $h(t) = \dot{f}(t)$. Based on Eq. (43), the linear second-order ESO may be formulated using the following equations [23]:

$$\begin{cases} \dot{z}_1 = z_2 + bu^* + d_1(y - z_1) \\ \dot{z}_2 = d_2(y - z_1) \end{cases} \tag{44}$$

where: $z_1 \approx y$; and $z_2 \approx f(t)$ are the estimation value of x_1 and x_2 ; d_1 and d_2 are the gain of the estimator, can be chosen as:

$$\begin{cases} d_1 = \beta_1\omega_0 \\ d_2 = \beta_2\omega_0^2 \end{cases} \tag{45}$$

Following Hurwitz's method, the values of β_1 and β_2 are chosen to satisfy the solutions of the equation $(s^2 + \beta_1s + \beta_2 = 0)$ must lie in the left half of the virtual plan [23]. So, the bandwidth of observer ω_0 is a parameter for turning the controller. Generally, the controller does not need an exact model of the system. It uses ESO to estimate disturbances and uncertainties so that the system can be controlled by a proportional controller as in Equation 45. The advantage of this control solution is that the exact model and parameters do not need to be found exactly. Finally, the control input is now predicated on the outputs of the ESO and is formulated as:

$$u^* = \frac{1}{\hat{b}}(-z_2 + \dot{p}_r - ks - \hat{E}sign(p_r - z_1)) \tag{46}$$

BENDING EXPERIMENT AND IDENTIFICATION

Figure 3 illustrates the design schematic, including the principal dimensions of the soft mechanism and the experimental model. The pneumatic soft finger in this study has three components: i) the main body, ii) the base, and iii) the air chamber. The suggested soft finger has the following dimensions: total length of $L_0 = 80$ mm, body cross-section dimension of $D = 32$ mm, air chamber length of $L_{air} = 70$ mm, base length of $L_b = 6$ mm, air chamber diameter of $d_{air} = 6$ mm and the base with diameter of $D_b = 38$ mm. The soft actuator in this study is made of silicone rubber (Dragon Skin 30) which is often utilized in soft mechanisms. The material exhibits an elongation at break of 364%, a density of 1070 kg/m^3 , and a shore hardness of $H = 30A$ and the poisson's ratio is $\mu = 0.49$ according to the data sheet [24]. The primary aim of this study is to model and regulate the pneumatic soft finger; hence, the specific design dimensions of the finger are not elaborated upon in this research. Figure 3 illustrates the experimental model employed to quantify the bending angle of the flexible mechanism in response to pressure, comprising a pressure regulating valve, a conventional straightedge, and the flexible mechanism itself. The pressure regulating valve is utilized to modulate the pressure of the compressed air delivered to the actuator. The purpose of this experiment is to investigate the bending angle θ according to the pressure value of the experimental sample; however, this bending angle value cannot be measured directly but must be measured indirectly through 4 marked points (1, 2, 3, 4) to measure the angles θ_1 , and θ_2 as can be seen in Figure 3. And, these angles are used to calculate the bending angle:

$$\theta = |\theta_1 - \theta_2| \tag{47}$$

A standard straightedge will be placed next to the sample during the experiment as a reference when used in *ImageJ* software [25]. The experimental sample with marked points is mounted to the support. Compressed air from the air compressor is connected to the fine-tuning pressure regulating valve, and the output of the regulating valve will be connected to the air chamber. The pressure will then be increased slowly, from 0 MPa, step by 0.02 MPa, allowing the sample to stabilize for 3 seconds and saving the image for measurement. Figure 4 illustrates the experimental outcomes of quantifying the bending angle of the soft mechanism in correlation with different pressures. Experimental results show that there is a correlation between bending angle and pressure.

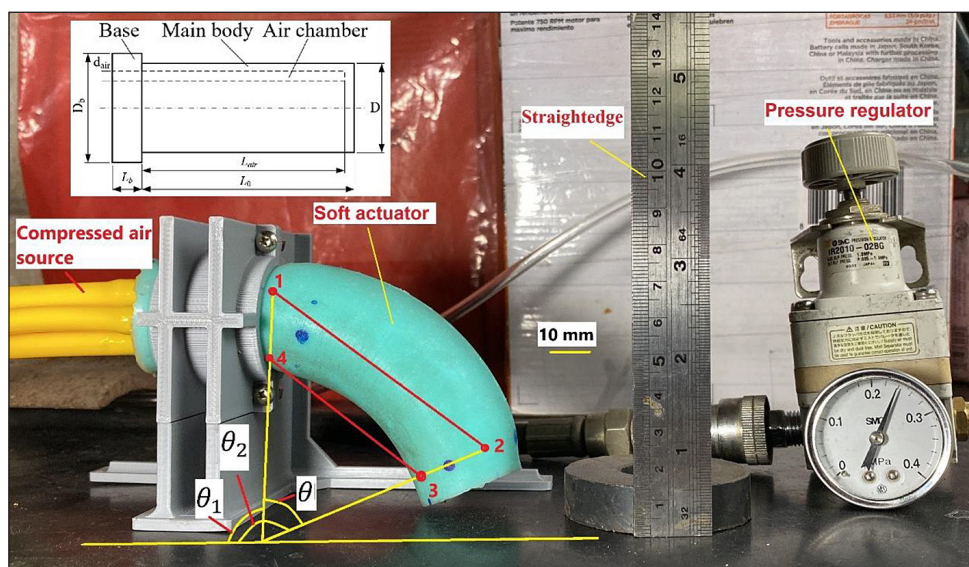


Figure 3. Bending angle at 24 kPa pressure

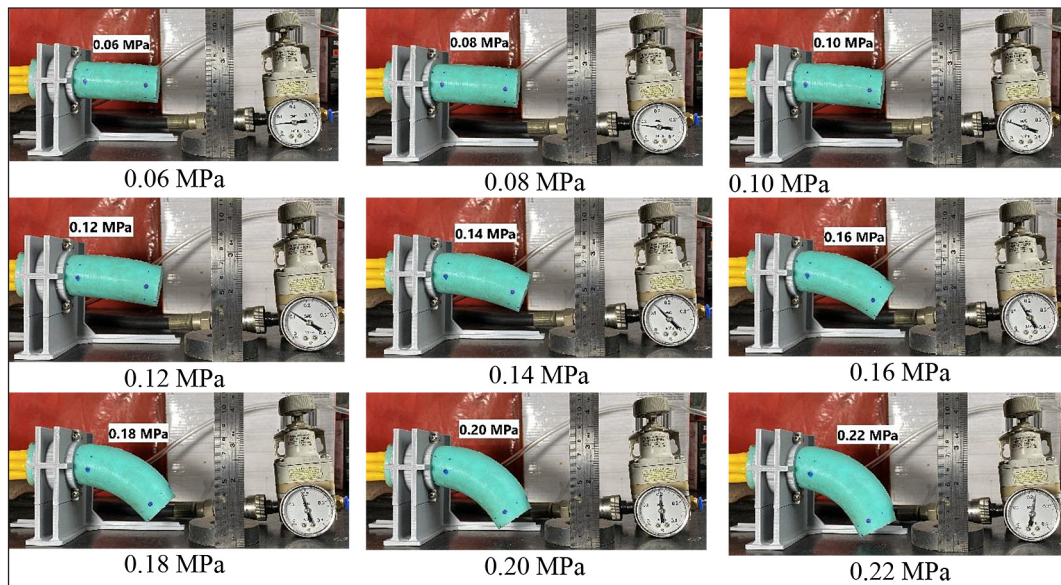


Figure 4. Experimental results of the correlation between bending angle and pressure

After the measurement process using *ImageJ* software, we get a table of results of measurement values of bending angle θ (degree) as shown in Table 1. The identification equations for the angular displacement of the air chambers are derived using MATLAB’s Curve Fitting Tool. As mentioned earlier in Equation 9, the identification equation chosen is the quadratic equation, as follows:

$$\begin{cases} \theta = 1176.96p^2 + 1.61p & p \geq 0.05\text{MPa} \\ \theta = 0 & p < 0.05\text{MPa} \end{cases} \quad (48)$$

The estimation results and experimental results between bending angle and pressure are presented in Figure 5. The high agreement between

Table 1. The experimental result of bending angle

Air pressure (MPa)	Number of measurements	Bending angle (degree)
0	4	0
0.06	4	4.281
0.08	4	8.191
0.1	4	10.221
0.12	4	17.01
0.14	4	21.275
0.16	4	30.634
0.18	4	39.901
0.2	4	46.989
0.22	4	54.484
0.24	4	68.077

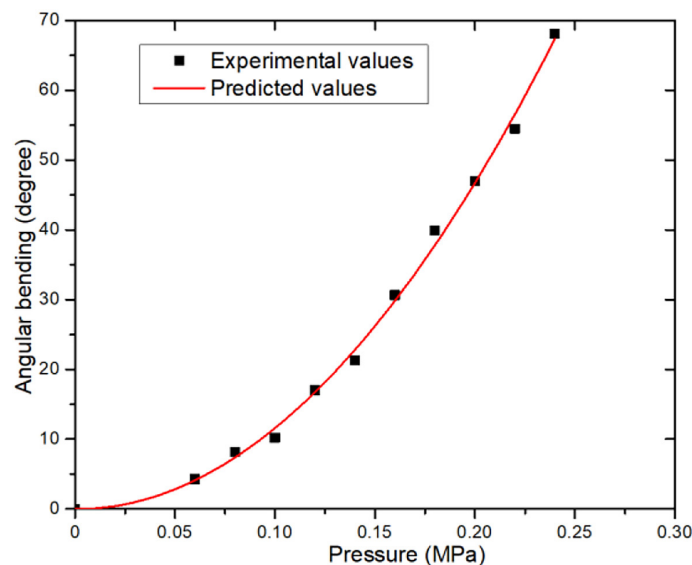


Figure 5. Experimental results and prediction of bending angle with pressure

the two results shows that the software structural model equations are highly reliable and accurate.

Figure 5 illustrates that when pressure levels vary from 0 MPa to 0.05 MPa, the bending angle diminishes to below 5 degrees. At a pressure of 0.05 MPa, the mean bending angle is 3.71 degrees. This suggests that the experimental sample has a minimal deformation amplitude, implying that the starting pressure levels must above the elastic deformation capacity of the sample. Once the pneumatic pressure sufficiently surpasses the elastic deformation threshold, the experimental sample exhibits considerable distortion with each pressure increment. Upon surpassing the elastic deformation threshold, with pressure values between 0.10 MPa and 0.24 MPa, the bending angle θ and pressure exhibit a roughly linear relationship.

The regression Equation 48 is quadratic, with the degree of freedom intersecting the origin at 0 MPa, indicating that at a pressure of 0 MPa, the experimental sample remains undeformed. With the R^2 value of Equation 48 being 0.9985, meeting the reliability condition ($\alpha = 0.05$), the quadratic regression equation is reliable and consistent with the experimental value.

The general control scheme for the soft finger in this paper is shown in Figure 6. From the relationship between pressure and bending angle obtained experimentally as shown in Equation 48, each bending angle value will find a corresponding required pressure. This desired pressure value is the input value of the pressure controller based on adaptive sliding mode and ESO control. The output of this controller is the condition to activate the ON/OFF pneumatic system valves. The mass flow rate of compressed air is supplied to the soft mechanism according to Equation 21. A pressure sensor will provide the actual pressure signal at the air chamber of the actuator to be the pressure signal feedback to the controller fulfilled its control function. The principal objective of the position servo control system is to effectively

direct the soft finger to attain a specific position within a defined range. The controllers do not directly regulate position, rather, positional control is a direct result of the regulated pressure applied in the air chamber. By this control, the bending angle of the soft mechanism is controlled without using a curvature sensor.

SIMULATION RESULTS

Simulations are developed with MATLAB/Simulink to evaluate the performance of the non-linear control and estimation algorithms. The initial volume of the compressed air chamber is. The coefficient k is equal to 1.4 because the air compression process is isothermal. The ideal gas constant $R_{special} = 287 (J \cdot K^{-1} \cdot mol^{-1})$, and the gas temperature is $T = 297 \text{ }^\circ K$. The coefficient is calculated according to .

The valve set for each chamber cannot be opened at the same time. This means that there are three possible states for each valve system: charge when mass flow is positive (K_1 open and K_2 closed), discharge when mass flow is negative (K_1 closed and K_2 open), and hold when both valves are closed. The pressure regulator valve adjusts the source pressure to 0.38 MPa. The controller parameters are selected manually as shown in Table 2.

Figure 7 illustrates the simulation results with input signals represented as steps, exhibiting equivalent amplitudes of 10° , 50° , and 20° with a step duration of 2 seconds. Figure 7a) illustrates the simulation outcomes of the angular displacement of the soft finger with step input. The controller’s ability to precisely monitor location is very good. The control effort can be further reduced, at the cost of slower response, by choosing lower values for the proportionality factor K . Figure 7b shows the desired pressure values interpolated from the reference bending angle and the pressure controlled in the pneumatic chamber.

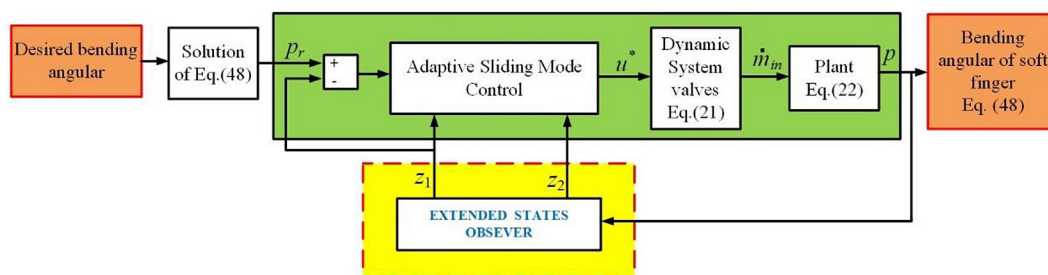


Figure 6. Control diagram of the soft finger

Table 2. Controller parameters

Model and controller parameters		
Parameters	Value	Unit
β_1	2	Dimensionless
β_2	1	Dimensionless
ω_0	1.6×10^4	Dimensionless
γ	1×10^{-3}	Dimensionless
k	6.8	Dimensionless

The results show that the tracking ability of the proposed controller is good. Clarify that the desired pressure is the pressure interpolated from the associated bend angle, while the air chamber pressure refers to the output pressure of the pressure controller.

The simulation results indicate that the response variation from the reference value is small, as seen in Figure 8a. The result is zoomed-in over the time interval for the finger to reach the equilibrium position from 1 s to 1.005 s as shown in

Figure 8b. The error compared to the reference value is approximately 0.05 degrees on average.

Figure 9 shows the simulation results of the mass flow rate into the air chamber according to the opening and closing state of the valves. The air flow increases correspondingly with larger bending angles of the soft finger as shown in Figure 9(a). The air flow rate supplied to the soft finger depends on the on/off status of the pneumatic valves K_1 and K_2 . Figure 9b illustrates the mass flow rate graph magnified over the interval from 0 s to 0.06 s. The mass flow simulation results also show that the opening and closing frequency of the pneumatic valve must be high to maintain the stable state of the system.

The paper simulates the sine response of the soft finger to show how well this controller works. The input is the sine wave with an amplitude of 20 (degrees), a frequency of 0.625 Hz, and a bias of 30 (degree). Figure 10(a) shows the results for the bending angle response, and Figure 10(b) shows the results for the pressure

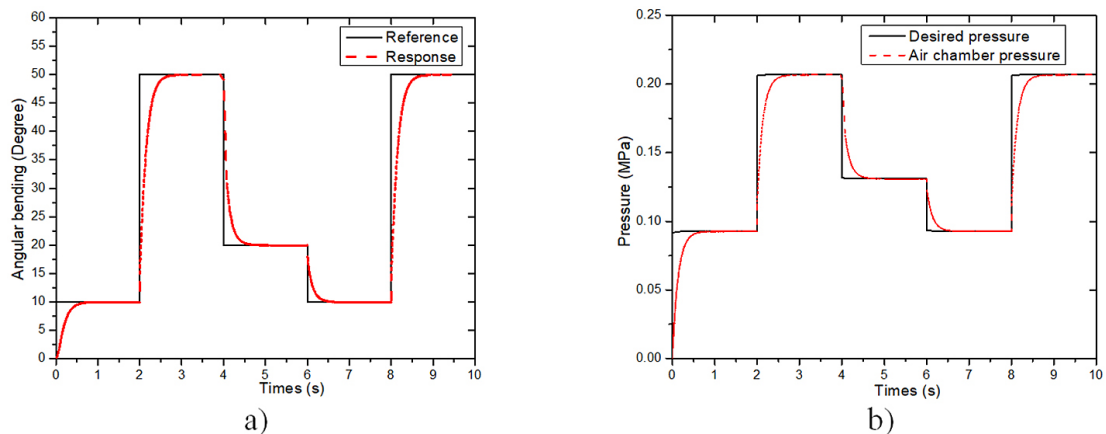


Figure 7. Simulation results of step response: (a) bending angle response, (b) pressure

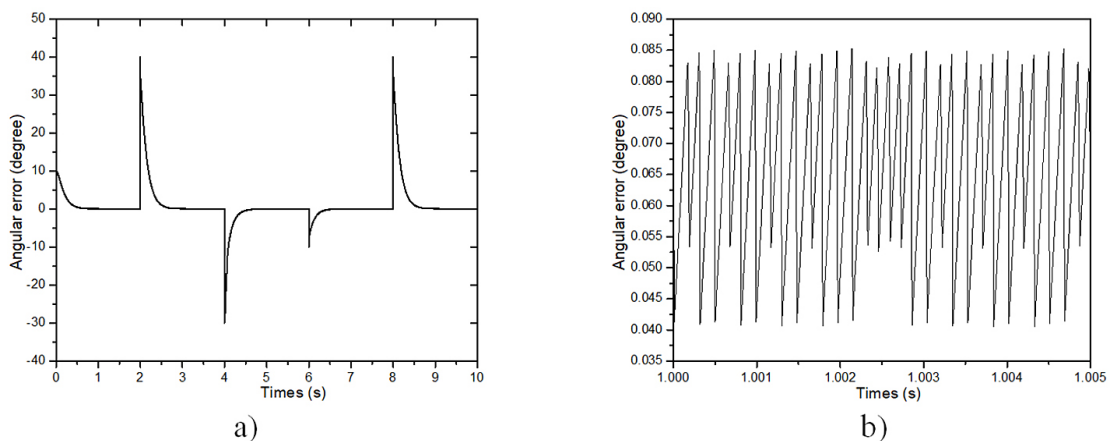


Figure 8. Simulation results of step response: (a) bending angle error, (b) zoomed-out

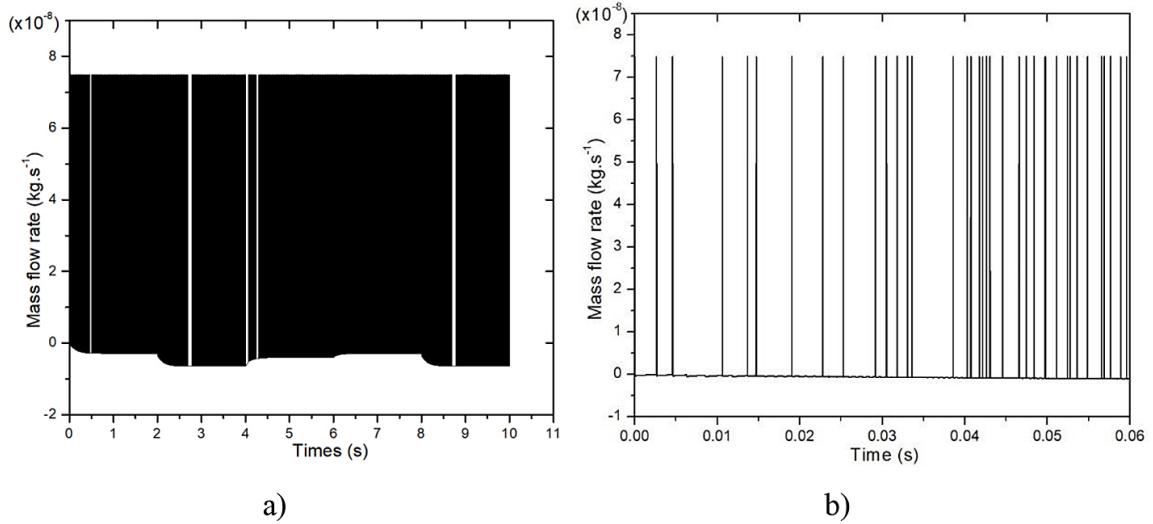


Figure 9. The mass flow rate into the air chamber: (a) mass flow rate, (b) zoomed-out

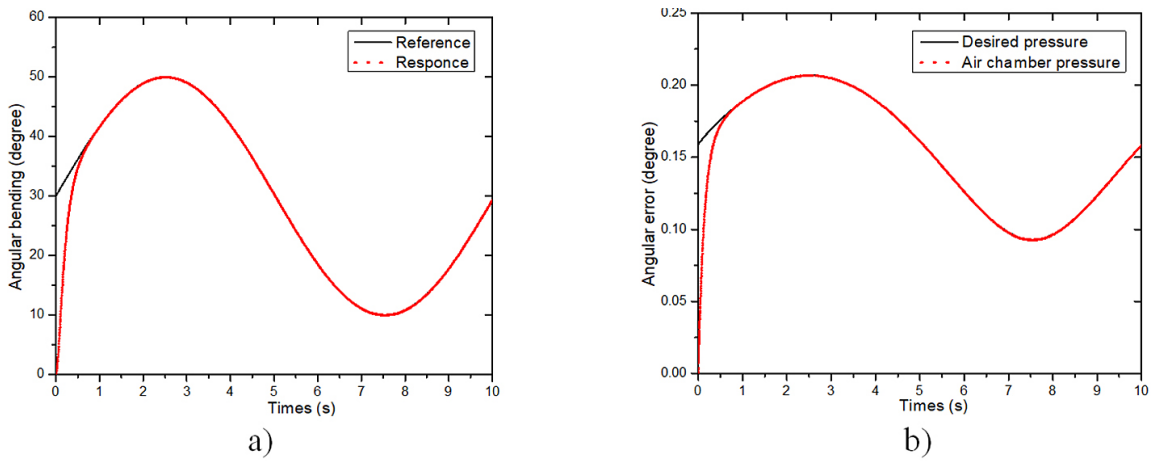


Figure 10. Simulation results of sine response: (a) bending angle response, (b) pressure

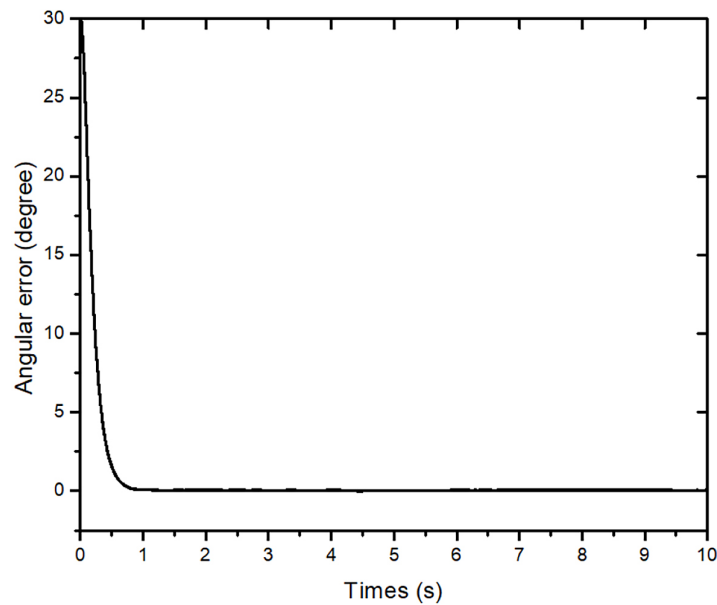


Figure 11. Simulation results for bending angle error of sine response

response. The simulation results have demonstrated a high tracking ability with this response. Figure 11 displays the static error of the sine response. This result also indicates that the controller has performed exceptionally well with the sine response, exhibiting a very small static error.

Consequently, we must assess the robustness of the proposed controller against external disturbance. An air leak is a common problem in a pneumatic actuator system. It may stem from a loose connection, a perforation in the tubing, or seal degradation, among other things. A sudden disturbance resembling an immediate air leak is introduced to the chamber pressure model at $t = 0.5$ s. The amount of disturbance can be calculated from the amount of gas leakage using the formula presented in previous section as:

$$d(t) = k \frac{R_{special} T}{V} (\dot{m}_{out}) \quad (49)$$

Let's assume that the gas volume of the soft finger at the moment of leakage is $V_d = (V_0 + 0.1V_0)$, indicating a 10% increase in the initial gas chamber volume. The simulation findings from Figure 9 lead us to assume that the amount of gas leakage is roughly 1% of the mass flow that the valves supply to the gas chamber, or $= 8E-10$ ($kg \cdot s^{-1}$). The controller parameters remain the same as above and the source pressure is 0.38 MPa. Figure 12 (a) illustrates the response of the control system to the disturbance. Despite the

disruption, the controller directs the soft finger to the specified places. Figure 12 (b) illustrates the simulation outcomes for the duration of up to 2 seconds. At time $t = 0.5$ s, a transient disturbance from gas leakage modifies the bending angle of the flexible mechanism. Nonetheless, the controller has effectively ensured the mechanism's stability while maintaining an acceptable static error. The steady static error is around 0.5 degrees. The static error arises due to the restricted mass flow rate through the pneumatic valves, which is insufficient to offset the mass flow loss from the actuator. Despite the adaptive controller's requirement for a high opening and shutting frequency of these valves, the orifice opening of these ON/OFF valves remains constant, hence constraining the mass flow rate. However, the pressure regulating valve can reduce this error by increasing the source pressure. The results presented Figure 13 support this conclusion. At a source pressure of 0.38 MPa, a gas leak at $t = 0.5$ s leads to a stable static inaccuracy of approximately 0.5 degrees, as illustrated in Fig. 12(b). Figure 13 demonstrates that elevating the source pressure to 0.42 MPa significantly reduces this inaccuracy within the same system. The elevated source pressure increases the mass flow rate through the pneumatic valve. This will create a balance between the airflow entering the soft mechanism. The simulation results indicate that the proposed method for regulating the bending angle of the soft finger through a pressure controller is entirely viable.

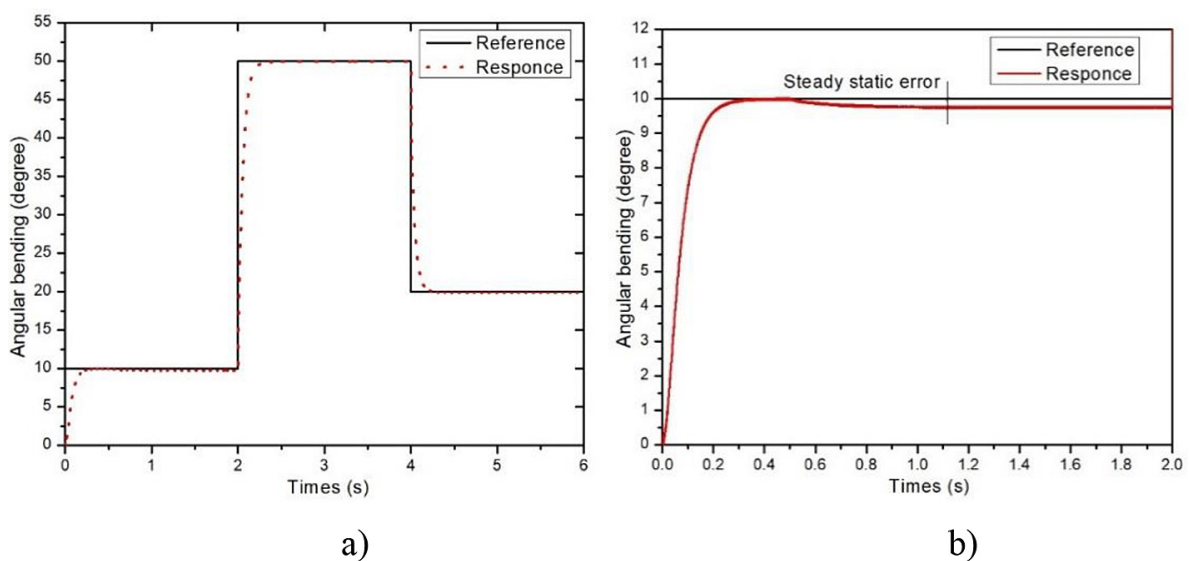


Figure 12. Simulation results of step response with disturbance with pressure source 0.38 MPa: (a) bending angle response, (b) zoomed-out

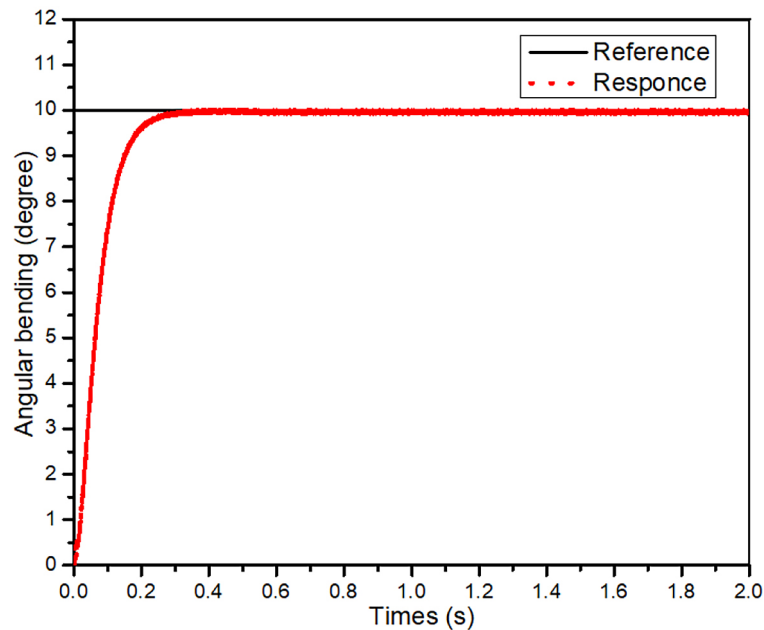


Figure 13. Simulation results of step response with disturbance with pressure source 0.42 MPa

CONCLUSIONS

This paper has developed a bending finger for use in pneumatic hand robot. The theoretical analysis of both the soft finger and the pneumatic valve have been fully developed. And, bending experiments to find the relationship between the bending angle and the air pressure have been carried out. The motion dynamics of the soft finger are modelled using a second-order function. Due to the nonlinear model, uncertainty and disturbance of the system, the controller, which is a combination of adaptive sliding mode and active rejection control has been adopted to track the change of the bending angle. The ESO was used to estimate the angular velocity state and the uncertainty vector across the entire state space. In order to verify the effectiveness of the controller, simulations under various desired bending angles have been performed. The simulation results show that there are small steady-state errors in the actuator response. However, this error is negligible and suitable for robot-hand applications. In the future, we plan to implement the control for a real pneumatic soft finger. We expect the experimental results to align with the simulation results in the paper.

Acknowledgements

The authors are very grateful for the support received from the Ho Chi Minh City University of Industry and Trade, and University of Technology

(HCMUT)-Vietnam National University Ho Chi Minh City for this research.

REFERENCES

1. Zaidi S, Maselli M, Laschi C, Cianchetti M. Actuation technologies for soft robot grippers and manipulators: A review. *Curr Robot Rep.* 2021; 2: 355–69.
2. Yin R, Yang B, Ding X, Liu S, Zeng W, Li J, et al. Wireless multistimulus-responsive fabric-based actuators for soft robotic, human–machine interactive, and wearable applications. *Adv Materials Technologies.* 2020; 5: 2000341.
3. Zhu M, Do TN, Hawkes E, Visell Y. Fluidic fabric muscle sheets for wearable and soft robotics. *Soft Robotics.* 2020; 7: 179–97.
4. Jin X, Feng C, Ponnamma D, Yi Z, Parameswaranpillai J, Thomas S, et al. Review on exploration of graphene in the design and engineering of smart sensors, actuators and soft robotics. *Chemical Engineering Journal Advances.* 2020; 4: 100034.
5. Kragic, D., Gustafson, J., Karaoguz, H., Jensfelt, P., and Krug, R. Interactive, collaborative robots: challenges and opportunities. In *IJCAI (2018, July)* 18–25.
6. Firth, C., Dunn, K., Haeusler, M.H., Sun, Y. Anthropomorphic soft robotic end-effector for use with collaborative robots in the construction industry. *Automation in Construction* 2022; 138): 104218.
7. Tlach V, Kuric I, Zajačko I, Kumičáková D, Rengevič A. The design of method intended for implementation of collaborative assembly tasks.

- Adv Sci Technol Res J. 2018; 12: 244–50.
8. Ebrahimi N., Bi C., Cappelleri D.J., Ciuti G., Conn A.T., Faivre D., et al. Magnetic actuation methods in bio/soft robotics. *Adv Funct Materials*. 2021; 31: 2005137.
 9. Pal A., Restrepo V., Goswami D., Martinez R.V. Exploiting mechanical instabilities in soft robotics: control, sensing, and actuation. *Advanced Materials*. 2021; 33: 2006939.
 10. Trivedi D., Lotfi A., Rahn C.D. Geometrically exact models for soft robotic manipulators. *IEEE Trans Robot*. 2008; 24: 773–80.
 11. Jeon H., Le Q.N., Jeong S., Jang S., Jung H., Chang H., et al. Towards a snake-like flexible robot with variable stiffness using an SMA spring-based friction change mechanism. *IEEE Robot Autom Lett*. 2022; 7: 6582–9.
 12. El-Atab N., Mishra R.B., Al-Modaf F., Joharji L., Alsharif A.A., Alamoudi H., et al. Soft actuators for soft robotic applications: a review. *Advanced Intelligent Systems*. 2020; 2: 2000128.
 13. Xavier M.S., Tawk C.D., Zolfagharian A., Pinskiar J., Howard D., Young T., et al. Soft pneumatic actuators: a review of design, fabrication, modeling, sensing, control and applications. *IEEE Access*. 2022; 10: 59442–85.
 14. Xie R., Su M., Zhang Y., Guan Y. 3D-PSA: A 3d pneumatic soft actuator with extending and omnidirectional bending motion. In: 2018 IEEE International Conference on Robotics and Biomimetics (ROBIO). Kuala Lumpur, Malaysia: IEEE; 2018; 618–23.
 15. Xavier M.S., Tawk C.D., Yong Y.K., Fleming A.J. 3D-printed omnidirectional soft pneumatic actuators: Design, modeling and characterization. *Sensors and Actuators A: Physical*. 2021; 332: 113199.
 16. Connolly F., Walsh C.J., Bertoldi K. Automatic design of fiber-reinforced soft actuators for trajectory matching. *Proc Natl Acad Sci USA*. 2017; 114: 51–6.
 17. Zhong G., Dou W., Zhang X., Yi H. Bending analysis and contact force modeling of soft pneumatic actuators with pleated structures. *International Journal of Mechanical Sciences*. 2021; 193: 106150.
 18. Polygerinos P, Wang Z, Overvelde JTB, Galloway KC, Wood RJ, Bertoldi K, et al. Modeling of soft fiber-reinforced bending actuators. *IEEE Trans Robot*. 2015; 31: 778–89.
 19. Roy R.C., Eric M.T. *Mechanics of Materials*. 4th edition. Wiley; 2020.
 20. Borgnakke C, Sonntag E.R. *Fundamentals of Thermodynamics*. 8th edition. Wiley; 2013.
 21. ISO 6358-2:2019 Pneumatic fluid power — Determination of flow-rate characteristics of components using compressible fluids. 2019.
 22. Slotine J-JE, Li W. *Applied nonlinear control*. Englewood Cliffs, N.J: Prentice Hall; 1991.
 23. Shao S., Gao Z. On the conditions of exponential stability in active disturbance rejection control based on singular perturbation analysis. *International Journal of Control*. 2017; 90: 2085–97.
 24. Dragon skin series, Available at https://www.smooth-on.com/tb/files/DRAGON_SKIN_SERIES_TB.pdf (2018/06/04)
 25. ImageJ. 2023. <https://imagej.net/ij/index.html>. Accessed 24 Dec 2023.